Chapter 3. Development of UWB GPR antennas

3.1. Introduction

Antennas may be the most critical point in an impulse GPR system, having a direct influence on its system performance. The antennas have to be specially designed to radiate pulses with given properties into the ground and transduce the backscattered signals from subsurface objects into a useful signal without too much affecting their shape.

They differ from conventional antennas in many aspects. First of all GPR antennas operate near the ground. The presence of the ground in the reactive field or near-field region of the antenna will influence the antenna characteristics. Secondly the antenna often operates in proximity to a second antenna, which gives an additional problem of antenna cross-coupling. Furthermore, the antenna transmits and receives fast transient electromagnetic signals with a large fractional bandwidth. A typical GPR could require an antenna with a fractional bandwidth of 100%. GPR antennas also should have a linear phase characteristic over this band, to limit the distortion of the emitted (or received) signal, and a constant polarisation with frequency.

All these supplementary requirements make that the number of antenna classes, which can be used, is limited. In some cases it also led to the design of new or modified antennas, matching the characteristics of the medium of propagation, the radiated signal and the system requirements.

In this chapter an overview of existing GPR antennas and ultra-wideband antennas will be given. Furthermore we will discuss some design goals of GPR antennas adapted for the application of demining. The design goals are mainly a product of field trials described in Chapter 2. Finally the development of TEM horn antennas for UWB GPR will be described.

3.2. Overview of existing GPR antennas

3.2.1. Conventional antennas

Nowadays, three main types of antennas are used in GPR applications: the element antennas, the frequency independent antennas and the horn antennas. A good overview of GPR antennas is given in [1].

Element antennas

Element antennas are the most widely used out of the three main types of antennas. Some examples of element antennas are the *monopole*, *dipole* and *bow-tie* antenna. This class of antennas is non-dispersive, and is characterised by linear polarisation, low directivity and some of them have a relatively limited bandwidth. The radiation characteristics of element antennas are well understood. The calculation of the radiated field is based on the approximation of the current distribution on the antenna by a number of elementary currents.

In the system configuration, the transmitting and receiving antenna can have either the same polarity (co-polarised) or an orthogonal polarity (cross-polarised), providing a lower antenna cross-coupling and eventually a better discrimination against certain man-made objects. Due to the low directivity, element antennas are used in close contact to the ground in order to couple as much energy as possible into the ground.

The latter has the disadvantage that the antenna impedance is influenced by the ground properties. Recently some research is done by TU-Delft to try to adapt the antenna to the ground properties [2].

Much effort has gone into techniques to extend the bandwidth of the element antennas. One possible solution is *resistively loading the dipoles*. The loading can be done either by an end loading, by a distributed loading or by a tapered resistive loading. Unloaded dipoles have internal reflections at the open end of the dipole. The resistive loading is essential in causing a rapid decay of current along the antenna to reduce the reflections at the antenna open ends, which results in less distortion or late-time ringing in the tail of the radiated transients. Hence a larger bandwidth is achieved. In 1965, Wu and King were the first to make a study on the tapered loading of a dipole antenna [3]. The profile for this resistive loading is known as the Wu-King profile. An overview of element antennas with resistive loading is given in [4]. Studies comparing a numerical finite difference time domain (FDTD) analysis with experimental measurements can be found in [5] and [6]. A disadvantage of the loading is the reduction of gain and radiation efficiency, although the latter is often considered less disadvantageous than antenna ringing. The radiation efficiency is defined as

$$\frac{energy\ radiated}{energy\ radiated + energy\ dissipated} \tag{3. 1}$$

and can in some cases drop down to 29% [6].

Another antenna that can be used as a wideband element antenna is the *bow-tie antenna* [7] (Fig. 3-1). This antenna is in fact a planar version of a finite biconical antenna, determined by a length L and an angle a. Bow-tie antennas, together with its many variants like shielded bow-tie, loaded bow-tie, tapered bow-tie etc., are probably the most popular among the element antennas. They can reach fractional bandwidths of 100% and more.
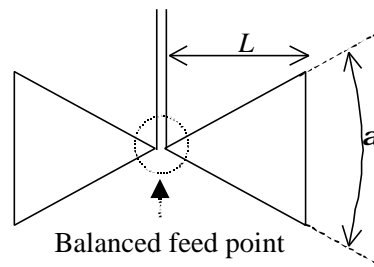
Fig. 3-1 : The bow-tie antenna.

Frequency independent antennas

A second main type of antennas used in GPR systems is the frequency independent antenna. An antenna is called frequency independent if it satisfies two principles: the scale principle and the truncation principle. It is known that antenna characteristics like pattern, impedance, etc., are invariant to a change of scale that is in proportion to the change in wavelength. If the shape of an antenna is entirely determined by angles, it would be invariant to a change of scale and hence, the performance of such an antenna would be independent of frequency. Furthermore the antenna has to satisfy the truncation principle, which implies that the current approaches zero at the end of an antenna. Otherwise truncation of the antenna has an effect on the pattern. In practise however, the dimensions of the antenna limit the lower frequency bound. A good overview of the subject is found in [8]. Examples of frequency independent antennas are the *log-periodic antennas* and the *spiral antennas*. An example of a spiral antenna is shown in Fig. 3-2. The formula for the spiral curve in polar co-ordinates is [8]

$$\boldsymbol{f} = \boldsymbol{f}_0 + \tan A \ \ln r \tag{3. 2}$$

which shows that the antenna is determined only by the angles $\boldsymbol{f}$ and A.
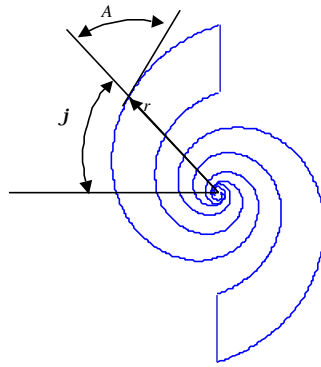
Fig. 3-2: Spiral antenna

A new member of the class of frequency independent antennas is the *Vivaldi antenna*. The Vivaldi antenna, introduced by Gibson in 1979 [9], consists of an exponential tapered slot line etched on a dielectric substrate (Fig. 3-3). The structure is usually fed by a micro strip, etched on the other side of the substrate (in dotted line on Fig. 3-3). The antenna characteristics are influenced by a number of parameters, like the dimensions and geometry of the slot line, the thickness and dielectric constant of the substrate, etc. The Vivaldi antenna is extremely wide-banded, bandwidths up to 5 octaves have been reported [9]. The lower cut-off frequency is limited by the dimensions of the antenna aperture. The antenna is characterised by a long electrical length for a reasonable short physical length, and therefore is an interesting antenna for GPR applications.
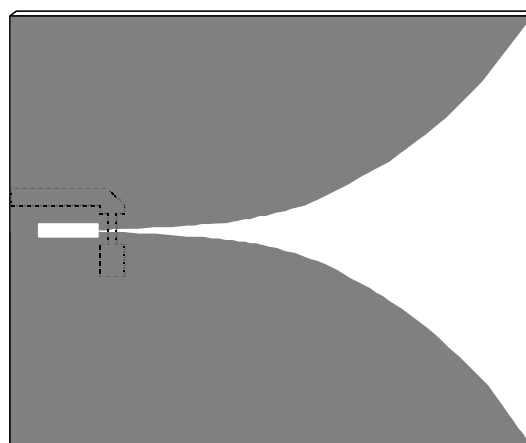
Fig. 3-3: Vivaldi antenna with micro strip feed

The frequency independent antennas however have the property of being dispersive. The impulse response of this class of antennas generally results in a chirp-waveform, which makes them unsuited for sending short pulses, as needed in time domain GPR. In stepped-frequency radar, the dispersive behaviour of the antennas can be compensated for. That is why they are only used in combination with this class of GPRs.

Horn antennas

The third main type of antenna is the *horn antenna*. Classical horn antennas have a fractional bandwidth around 66%, which is normally not enough for a GPR. Larger bandwidths are achieved with double-ridged horns. Horn antennas have the advantage of being directive. This means horn antennas can be used off ground. Examples of commercially used horn antennas are the 1GHz and the 2.5 GHz antenna of GSSI. They were originally developed for road inspection and can be mounted on a vehicle. The disadvantage of this kind of antenna is the size. Usually horn antennas are too large what makes them not user-friendly in rough terrain (*e.g.* the 1GHz antenna of GSSI are 102 cm * 22 cm* 32 cm).

3.2.2. Non-dispersive Ultra-wideband antennas

Thanks to the considerable progress in signal generators and receivers the last decades, the time domain UWB radar has won in interest. The main goal was to achieve higher spatial resolution, an easier target information recovery and a lower probability of interception. In this kind of application it is important that fast electromagnetic transients are radiated, without too much distortion. Therefore non-dispersive UWB antennas are needed, with a fractional bandwidth of 120% or greater. In one of the previous paragraphs we already mentioned the resistive loaded bow-tie antenna, which indeed can be classified in the family of UWB antennas. However if more radiation efficiency and directivity are pursued, the solution must be found in other types of antennas, mostly travelling wave antennas. An antenna is called a travelling wave antenna if the length of the antenna plates is several times larger than

the pulse lengths of the feeding signal. This means the wave actually travels along the antenna plates before it is radiated when reaching the end of the plates.

The *infinitely long biconical antenna* is an ideal radiator for fast electromagnetic transients [10][11][12]. Since its length is infinite and its shape is invariant to a change of scale, the infinitely long biconical antenna is a frequency independent antenna. The infinite biconical antenna is equivalent to a transmission line, guiding a spherical TEM wave. Its characteristic impedance and hence the antenna impedance is only function of q_0 (see Fig. 3-4). In practical use however, the antenna will have a finite length, so that reflections at the antenna end will occur. These unwanted reflections can, just like with the element antennas, be reduced by including resistive material in the antenna structure [13]. Fig. 3-4 shows a finite conical monopole antenna on a ground-plane.
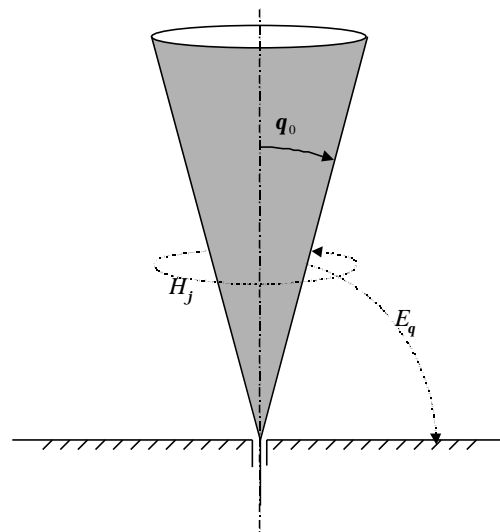
Fig. 3-4 : Conical monopole antenna of finite length on a ground-plane

A second type of UWB antenna, based on the biconical antenna is the *travelling wave TEM horn*. A travelling wave TEM horn consists of a pair of triangular conductors forming a V structure (Fig. 3-6), guiding essentially a TEM mode between its antenna plates. The TEM horn is studied in detail in Section 3.4.

A last type of UWB antenna is the *Impulse Radiating Antenna* (IRA). The IRA antenna is a parabolic antenna with a conical TEM transmission line as primary

source. The conical transmission line will launch essentially a spherical TEM wave towards the reflector. Suppose a step voltage is applied in the feed point of the transmission line. An observer on axis and in the far field of the antenna will first see a pre-pulse, due to the direct (backward) radiation of the feeding transmission line. This is followed by an impulse of short duration and high amplitude. The impulse is proportional to the first temporal derivative of the step on the feeding transmission line. The main impulse is followed by a tail due to reflections on the transmission line end and associated with low frequency components of the feeding signal. These reflections are limited by putting resistors between the transmission line and the reflector. The IRA antenna is represented on Fig. 3-5. This type of antenna is conceived and studied by C.E. Baum and E.G. Farr. More details can be found in [14][15][16].
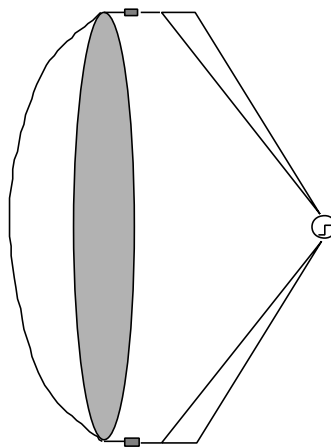
Fig. 3-5: The Impulse Radiating Antenna

3.3. GPR antenna design goals for the demining application

As already mentioned in Chapter 2, most GPR antennas are designed for applications other than the demining application and do not meet the specific requirements as needed for the demining application. From the experience obtained by the field trials and taking into account the UWB approach, five technical and practical design goals for UWB antennas are set:

1. The antenna must be able to radiate or receive fast electromagnetic transients with a spectrum between 500 MHz and 4.5 GHz

2. The antenna must be usable off ground, not only for safety reasons but also to improve the mobility of the detector. As a consequence, the antenna must have a high directivity so that it can still couple sufficient energy into the ground to achieve a penetration depth of 20 cm in any soil

3. The antenna must guarantee a high degree of mobility, having an implication on the dimensions and weight of the antenna. Minefields have often a rough surface and are covered with a lot of vegetation. Only little antennas can guarantee a sufficient flexibility in such a scene. Little antennas are also better for hand-held applications

4. The antenna properties must be independent of the ground properties. The influence of the ground will be reduced when using the antenna off ground

5. The antenna must be cheap in production to limit the overall cost of the sensor. This will always be asked for in the case of *humanitarian* demining.

One of the most promising antennas that can meet these design goals, is the travelling wave TEM horn. Therefore we have chosen this type of antenna as the starting point for our study.

3.4. Air-filled TEM horn

3.4.1. TEM horn antennas

In an effort to increase the directivity or the antenna gain for a broadband and non-dispersive antenna, many researchers have considered a TEM horn. A travelling wave TEM horn consists of a pair of triangular conductors forming a V structure (Fig. 3-6), capable of radiating and receiving a fast transient pulse [4]. It is assumed that the TEM horn guides essentially the TEM mode within the frequency range of interest by maintaining a constant characteristic impedance and that, by neglecting the edge diffraction effect and fringe fields, a linearly polarised spherical wave is radiated. The

operation of a TEM horn is fairly simple. On transmission, the TEM horn radiates a signal that is proportional to the first time derivative of the incident voltage pulse in the feeding point. On reception, the horn outputs a voltage pulse that has the same shape as the incoming electric field (a detailed explanation for this is given in Chapter 4, Section 4.3.3). A conventional TEM horn is completely characterised by three parameters:

- L the length of the antenna plates,
- j_0 the azimuth half-angle,
- q_0 the elevation half-angle.

The characteristic impedance of an infinite long TEM horn (L=∞) is only function of the two angles j_0 and q_0. Theoretically a TEM mode does not have an upper cut-off frequency. In practice however some higher modes exist and will introduce an upper cut-off frequency. The dimension L of the antenna mainly governs the lower cut-off frequency.
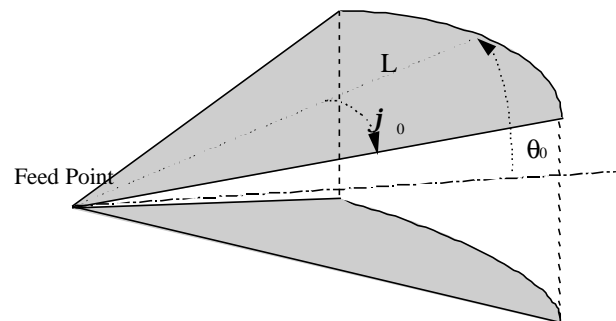
Fig. 3-6: The travelling wave TEM Horn

The conventional design of the TEM horn is based on the infinitely long biconical antenna. Many variants are possible, *e.g.* resistive loading of the antenna [17], tapering the antenna plates [18], gradually changing the separation angle between the antenna plates [19], or placing a dielectric lens at the aperture [20].

There is until now no exact theoretical analysis of this structure available. Various approximate analyses and models have been made to allow the antenna design.

The antenna impedance

To calculate the antenna impedance and the surge impedance along the antenna plates, two methods are often found in literature. Both models are based on the approximation that the antenna is infinitely long. In this case, the antenna is equivalent to a conical transmission line. Suppose the origin of co-ordinates in the feed point (apex) of the antenna. For a given value of the two angles j_0 and q_0, the characteristic impedance of the transmission line is constant, independent of the radial co-ordinate r. Hence, the antenna impedance (for $r \rightarrow 0$), and the surge impedance will then be equal to the characteristic impedance of the transmission line. The surge impedance is defined as the impedance measured in any point of the antenna by means of a step excitation. It does not take into account the backward waves due to reflections at the antennas open end, arriving later.

The characteristic impedance of the transmission line can be found by conformal mapping. In a first step, the two plates are projected by a stereographic projection into two plates of circular arcs. In a second step, the characterisric impedance of the circular arc problem is solved by a standard method of conformal mapping [10][21]. The results are usually given in tables and curves as a function of the two angles j_0 and q_0. This method of conformal mapping can also be used to calculate the field distribution between the antenna plates [22].

A second approach used for the calculation of the characteristic impedance of the infinite TEM horn is based on cascading sections of strip-lines [18][23]. The antenna is split into electrically small segments along its length (Fig. 3-7). Each segment of the antenna is approximated by a parallel twin line and the antenna is modelled as a collection of those parallel twin lines in serie.

(a) Side view   (b) Front view of one section
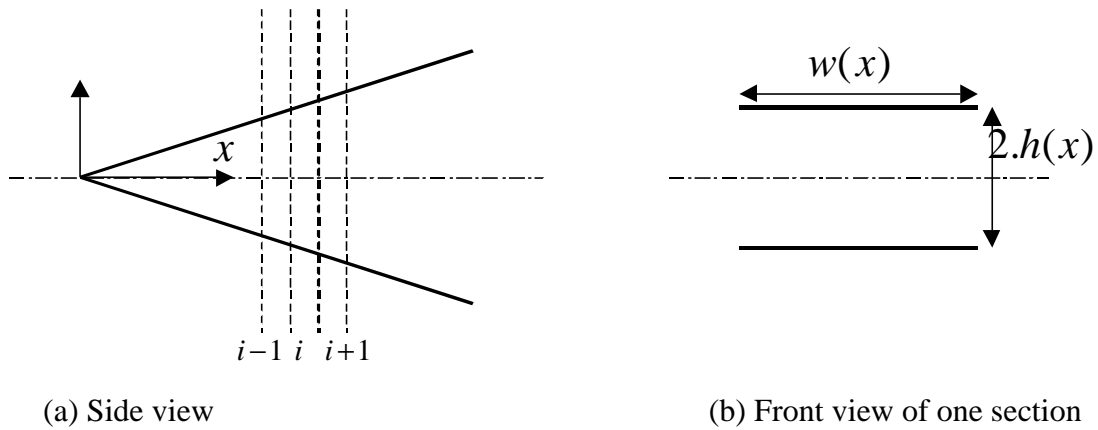
Fig. 3-7 : TEM horn as a cascade of strip lines

The characteristic impedance of such a twin line segment is calculated as two times the characteristic impedance of a micro-strip of height h and width w in the absence of a dielectric. The characteristic impedance of the micro-strip can be calculated for a given ratio w/h using the approximated expressions of Hammerstad and Jensen [24].

For a given value of the angles j_0 and q_0, the ratio w/h is constant and the characteristic impedance of each twin line segment will be the same, hence the surge impedance of the TEM horn will be constant.

The radiated far field

The evaluation of the far field, radiated by a TEM horn, can be done in the frequency domain as well as directly in the time domain. In the frequency domain approach the field is first calculated at the TEM horn aperture, as the field of the TEM mode that would exist in a horn of infinite length. Based on the assumption that the edge diffraction and the fringing field effects are neglected, the spherical field at the horn aperture is given in [4] as

$$E_y(x', y', 0) = \frac{r_0^2}{\sqrt{r_0^2 + x'^2 + y'^2}} \frac{e^{-jk\sqrt{r_0^2 + x'^2 + y'^2} - r_0^2}}{\sqrt{r_0^2 + y'^2}} \qquad \textbf{(3. 3)}$$

The origin of co-ordinates is taken in the middle of the antenna aperture (Fig. 3-8). The co-ordinates in the antenna aperture are indicated by primes and r_0 is the distance between the apex and the centre of the aperture. Huygen's principle is used with this field to predict the radiated field outside the aperture.
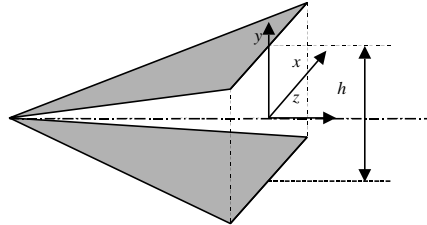
Fig. 3-8: Representation of co-ordinate system

A simple time domain model for the TEM horn is given in [25]. In this model, the antenna is considered as an open circuited transmission line. It consists of approximating the antenna by a succession of electric and magnetic dipoles, and summing their contributions. The model is simple but useful to help in the design of a TEM horn or to make comparisons with other antennas. If a step voltage of V_0 is applied at the antenna feed, the radiated electric field on boresight at a distance z is given by

$$E_y(z,t) = -\frac{V_0}{z}\frac{h}{2pcf_g}\left[d(t-\frac{z+r_0}{c}) + \frac{c}{2r_0}\left[-u(t-\frac{z+r_0}{c}) + u(t-\frac{z+3r_0}{c})\right]\right] \quad \textbf{(3. 4)}$$

with h the distance between the two antenna plates at the aperture (Fig. 3-8), c the speed of light, $f_g = Z_c / Z_0$ the geometrical impedance factor, Z_0 the impedance of free space, Z_c the characteristic impedance of the TEM horn, r_0 the distance between the antenna apex and the origin of co-ordinates and $u(t)$ the unit step function. Fig. 3-9 shows the graphical representation of the step response given by (3.4). The author also suggests a correction of the model for high frequencies [25].

E_y

Impulse area $= \dfrac{V_0}{z} \dfrac{h}{4pcf_g}$

0

t

$-\dfrac{V_0}{z} \dfrac{h}{8pr_0 f_g}$

$2r_0/c$

$t = \dfrac{z + r_0}{c}$
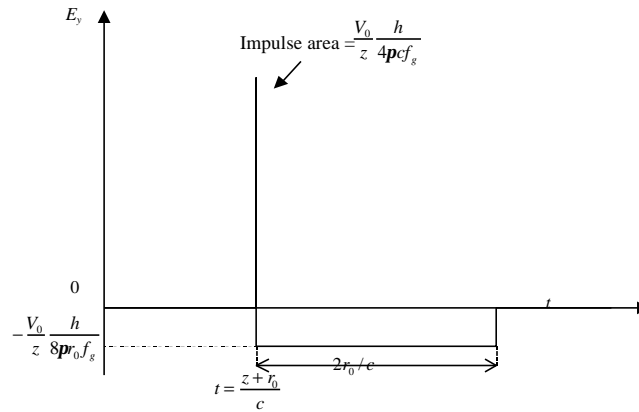
Fig. 3-9: Step response on boresight of TEM horn

Another possibility of calculating the antenna impedance and the radiated field are by numerical modelling of the TEM horn using the method-of-moments [4] or finite-difference time-domain (FDTD) code. Some didactic simulations of TEM horns using FDTD are found in [18].

3.4.2. Study of the wire Model

An accurate model of the TEM Horn is found in the wire method, where the antenna plates are replaced by a set of infinitely thin wires. The model was originally developed for the electromagnetic performance analysis of Electro-Magnetic Pulse (EMP) simulators [26][27], but can be used as a model for the air-filled TEM horn. The wire method is a time-domain-based method. The transient electromagnetic field emitted by a TEM horn antenna is considered to be the sum of the transient electromagnetic fields emitted by each individual wire.

The advantage of the wire model is that it provides at the same time an analytic expression for the early time radiated far field as for the surge impedance. Furthermore, the expressions of the far field and the antenna impedance are simple which makes them convenient for simulations and design purposes.

In the model the following assumptions are made. The current on the antenna plates is strictly radial and travels with the speed of light. As we are only interested in the TEM

mode of the antenna, this is an acceptable approximation. Furthermore we assume that the waveform and amplitude of the travelling current is constant along the wire, that the wires are infinitely thin and that the current is totally absorbed at the end of the antenna. In reality however a part of the current will bounce back at the antenna-end towards the feed point of the antenna. This phenomenon will cause late time ringing in the antenna, which will be omitted in this approach.

The radiation by one wire

In a first step the field radiated by a wire of length L is studied. The geometry of the wire and the associated co-ordinates are shown in Fig. 3-10. The co-ordinates on the wire are indicated with a prime.
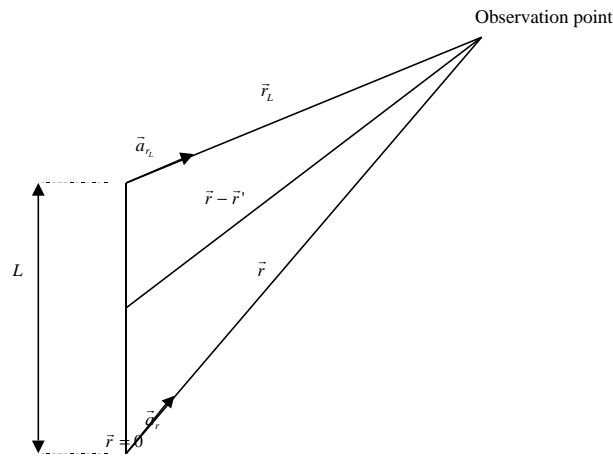
Fig. 3-10: Co-ordinate system for the study of the wire

Suppose a current pulse $I_{wire}(t)$ is applied at the wire at $\vec{r} = 0$. The radial current distribution on the wire is then

$$I(r',t) = I_{wire}(t - \frac{r'}{c}) \tag{3. 5}$$

with $r' = |\vec{r}'|$. The radiated electric field can be written as

$$\vec{E}(\vec{r},t) = -\vec{\nabla} f(\vec{r},t) - \frac{\partial \vec{A}(\vec{r},t)}{\partial t} \tag{3.6}$$

with $\vec{A}(\vec{r},t)$ the vector potential and $f(\vec{r},t)$ the scalar potential given by

$$\frac{\partial f(\vec{r},t)}{\partial t} = -c^2 \vec{\nabla}.\vec{A}(\vec{r},t) \tag{3.7}$$

For a wire of length L, the vector potential is written as

$$\vec{A}(\vec{r},t) = \left[\frac{m_0}{4p} \int_0^L \frac{I_{wire}(t - r'/c)}{|\vec{r} - \vec{r}'|} dr' \right] \vec{a}_{r'} \tag{3.8}$$

with $\vec{a}_{r'}$ the unit vector along the wire.

After substitution of (3.7) and (3.8) in (3.6), the electric field radiated by one wire $\vec{E}_{wire}(\vec{r},t)$ can be calculated [26] and is expressed as

$$\vec{E}_{wire}(\vec{r},t) = -\frac{1}{4pe_0} \left\{ \frac{\vec{a}_r}{r^2} q(t - \frac{r}{c}) - \frac{\vec{a}_{r_L}}{r_L^2} q(t - \frac{L + r_L}{c}) \right\}$$

$$\tag{3.9}$$

$$-\frac{Z_0}{4p} \left\{ \frac{\vec{a}_{r'} - \vec{a}_r.(\vec{a}_{r'}.\vec{a}_r)}{r(1 - \vec{a}_{r'}.\vec{a}_r)} I_{wire}(t - \frac{r}{c}) - \frac{\vec{a}_{r'} - \vec{a}_{r_L}.(\vec{a}_{r'}.\vec{a}_{r_L})}{r_L(1 - \vec{a}_{r'}.\vec{a}_{r_L})} I_{wire}(t - \frac{L + r_L}{c}) \right\}$$

with $r = |\vec{r}|$, $r_L = |\vec{r}_L|$ the distance between the observation point and the end of the wire, Z_0 the impedance of free space, and q the charge on the wire given by

$$q(t) = \int_0^t I_{wire}(t)dt \qquad \textbf{(3. 10)}$$

For a better insight of the radiation by a wire, we show in Fig. 3-11 some snapshots of the radiated field of one wire on a ground-plane. The snapshots are calculated on a 2mm by 2mm grid using equation (3.9). The vertical oriented wire, shown in white on the snapshots, has a length L of 10 cm. The feed point of the wire is downwards. In the simulation, the excitation current is a Gaussian pulse with a full width at half maximum (FWHM) of 40 ps. If $t_a = L/c$ is the time for the current to travel towards the end of the wire, the snapshots are given at $t = 0.5t_a$, $t = t_a$, $t = 1.5t_a$ and $t = 2t_a$. In each snapshot, the electric field is represented in magnitude.
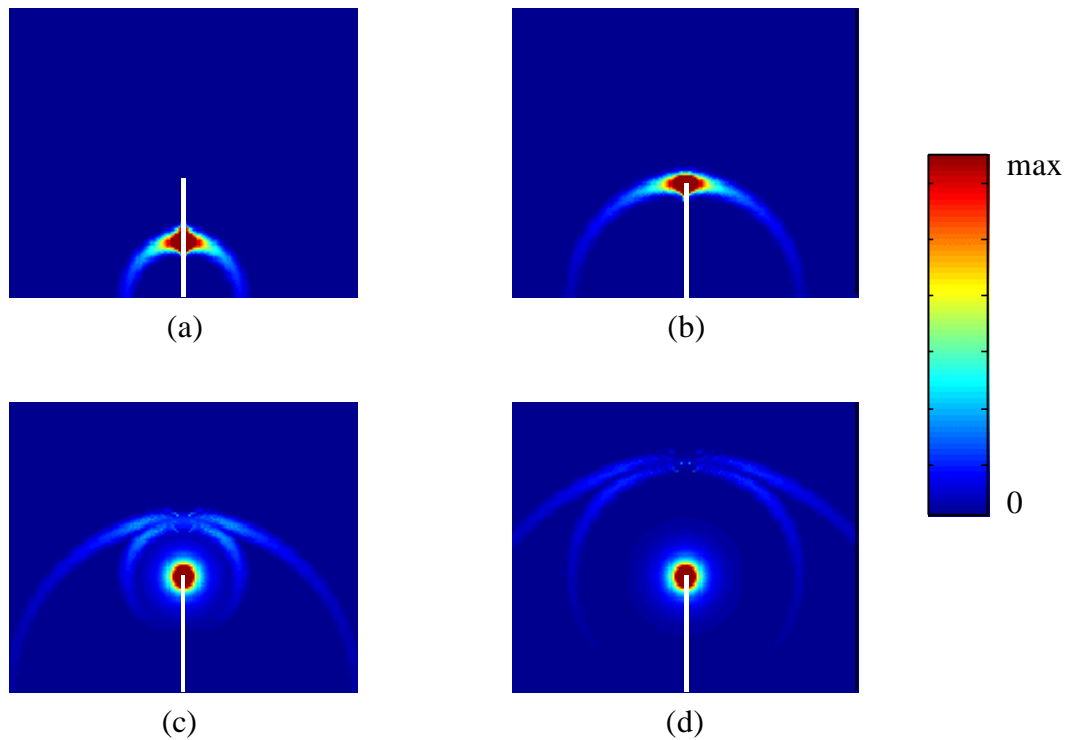
Fig. 3-11: Magnitude of the radiated electric field by one wire on a ground-plane. Snapshots taken at

(a) $t/t_a = 0.5$ (b) $t/t_a = 1$

(c) $t/t_a = 1.5$ (d) $t/t_a = 2$

On the snapshots we see that a first spherical wave, centred at the feed point $\vec{r} = 0$, is produced when the current pulse enters the wire. A second spherical wave, centred at $\vec{r}_L = 0$ is produced when the current reaches the open end of the wire. Because the second wave corresponds with a deceleration of charges, it will have a field opposite to the first wave. This is however not visible on the snapshots because only the field magnitude is shown. The electric field concentrated around the wire end in snapshot (c) and (d) is a static electric field due to the accumulated charges at the open end of the antenna. The charges stay there because in the model the current is absorbed at the wire end. In (3.9) it can be seen that this static field decreases with $1/r_L^2$.

A similar analysis in the time domain of the radiated electric field by a wire is found in [28], providing a good physical understanding of radiation phenomena.

The current distribution on the antenna plate

In a next step the current distribution on the antenna plate is considered. The geometry of the antenna plate and the associated co-ordinates are shown in Fig. 3-12. Suppose that a total current $I_0(t)$ is applied at the antenna feed and that the antenna plate is infinitely thin.
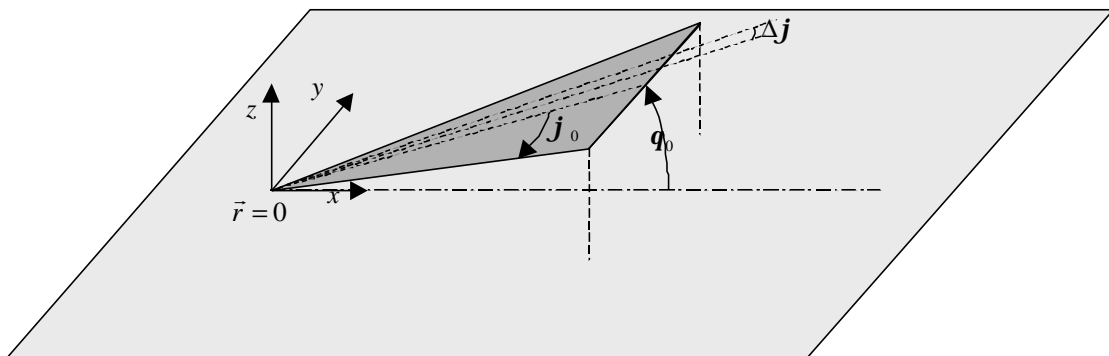
Fig. 3-12: The geometry of the antenna plate and the associated co-ordinates

In this case, the current on the plates can be considered as a radial directed current surface density $\vec{J}_S(\vec{r}',t)$. The co-ordinates on the plate's surface S are indicated with

a prime. The radial distribution of the current surface density is dictated by $I_0(t - |\vec{r}'|/c)$. The azimuth distribution of the current surface density is governed by a function $F(\boldsymbol{j}, \boldsymbol{j}_0)$. According to the current distribution on a micro strip, the current azimuth distribution function is taken [26]

$$F(\boldsymbol{j}, \boldsymbol{j}_0) = \frac{1}{\boldsymbol{p}\sqrt{\boldsymbol{j}_0^2 - \boldsymbol{j}^2}} \qquad \textbf{(3. 11)}$$

Note that the current azimuth distribution function is normalised, so that

$$\int_{-\boldsymbol{j}_0}^{\boldsymbol{j}_0} F(\boldsymbol{j}, \boldsymbol{j}_0)d\boldsymbol{j} = 1 \qquad \textbf{(3. 12)}$$

Fig. 3-13 shows a plot of the azimuth distribution function for $\boldsymbol{j}_0 = 30°$. We notice that the current surface density will be more important near the side edges of the antenna plate.
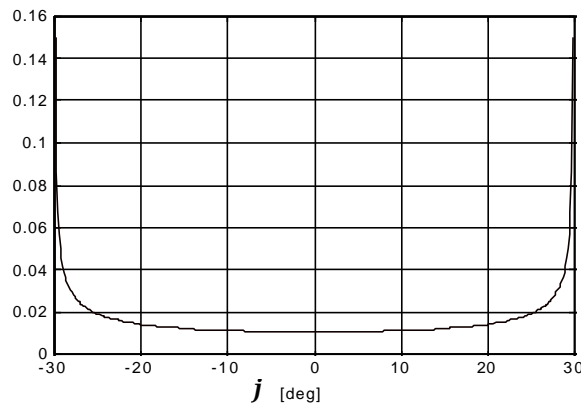
Fig. 3-13 : Azimuth current distribution function on the antenna plate

Total field radiated by the TEM horn

In the next step, the antenna plate is replaced by a mesh of N radial wires with a common apex. Each wire i is characterised by an azimuth angle

$$\boldsymbol{j}_i = (i - \frac{1}{2})\Delta\boldsymbol{j} - \boldsymbol{j}_0 \qquad i = 1,2,...N \qquad \textbf{(3. 13)}$$

with

$$\Delta\boldsymbol{j} = \frac{2\boldsymbol{j}_0}{N} \qquad \textbf{(3. 14)}$$

and an elevation angle

$$\boldsymbol{q}_i = \arcsin(\sin\boldsymbol{q}_0 \cos\boldsymbol{j}_i) \qquad \textbf{(3. 15)}$$

The current in wire i is given by

$$I_{wire,i}(t) = I_0(t). \int_{\boldsymbol{j}_i - \Delta\boldsymbol{j}/2}^{\boldsymbol{j}_i + \Delta\boldsymbol{j}/2} F(\boldsymbol{j},\boldsymbol{j}_0)d\boldsymbol{j} \qquad \textbf{(3. 16)}$$

Finally the total field radiated by the TEM horn is obtained by summing the field expression from each individual wire with its current:

$$\vec{E}_{Tot}(\vec{r},t) = \sum_{i=1}^{N} \vec{E}_{wire,i}(\vec{r},t) \qquad \textbf{(3. 17)}$$

Note that, as each wire in the TEM horn has an image wire with an oppositely directed current, all the terms involving the charges $q(t - r/c)$ are cancelled out.

In Fig. 3-14 a simulation of a TEM horn is shown using the wire model. The antenna has a length L of 10 cm, $j_0 = 25°$ and $q_0 = 10.2°$. In the four snapshots the xz-plane is represented (see Fig. 3-12). The intersections of the antenna plates with the xz-plane are shown in white. At $t = 0\,s$ a Gaussian current pulse (the same as in the previous simulation with the single wire) is applied at the antenna feed point. The snapshots are given at respectively $t = 0.5t_a$, $t = t_a$, $t = 1.5t_a$ and $t = 2t_a$, with t_a the time for the current pulse to reach the end of the antenna plates. The magnitude of the electric field is in each snapshot re-scaled and plotted on a colour scale.

(a)

(b)

(c)

(d)
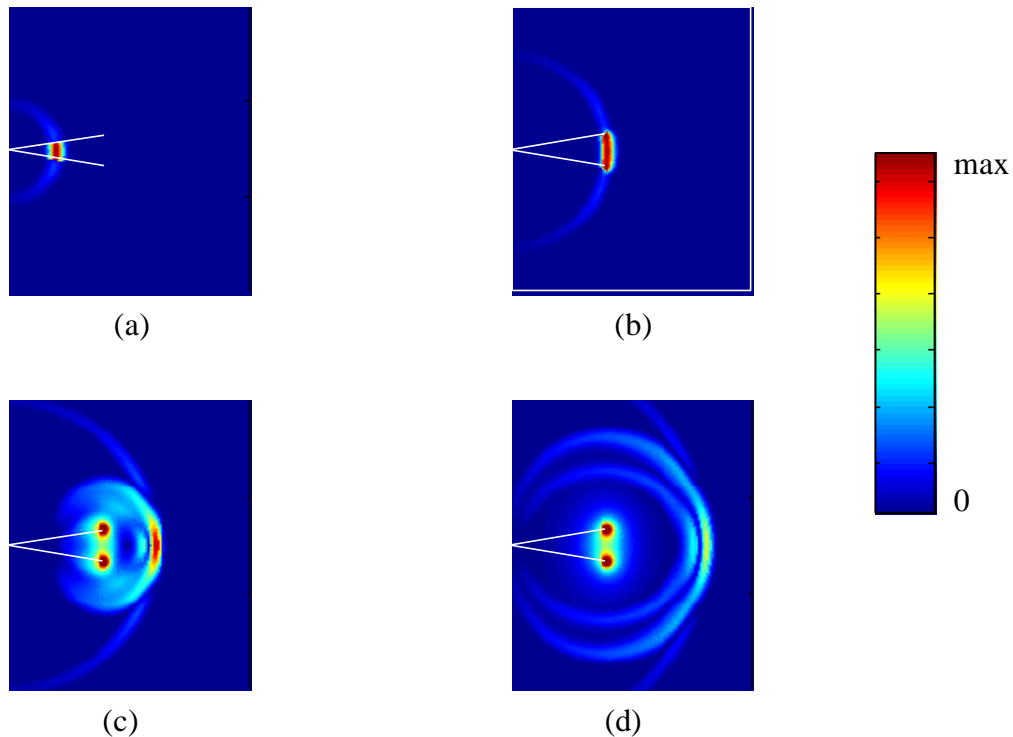
Fig. 3-14 : Magnitude of the radiated electric field in the xz-plane by a TEM horn. Snapshots taken at

(a) $t / t_a = 0.5$ (b) $t / t_a = 1$

(c) $t / t_a = 1.5$ (d) $t / t_a = 2$

On snapshot (a) and (b) we see the pulse-shaped wave travelling between the antenna plates. Note the wave on the outside of the antenna plates. This is also a spherical

wave centred at the antenna feed, but with an electrical field opposite to the one inside the antenna (the sign is not visible on the snapshots because the magnitude of the field is plotted). This wave is important to explain the negative "pre-pulse" radiated by the dielectric-filled TEM horn (see Section 3.5). It is also at the origin of the pre-pulse encountered by the IRA antenna. On snapshot (c) and (d) the static electric field at the antenna end, due to the accumulation of charges, is visible.

The field radiated on boresight (in the x-direction) has the shape of the first time derivative of the current pulse (this can not be seen in previous figure, as only the magnitude of the field is represented). To show this we plot in Fig. 3-15 the normalised E_z component of the electric field as function of time in a point on the x-axis at 30 cm from the antenna feed. In Fig. 3-15 (a) the Gaussian current pulse is represented.

(a)

(b)
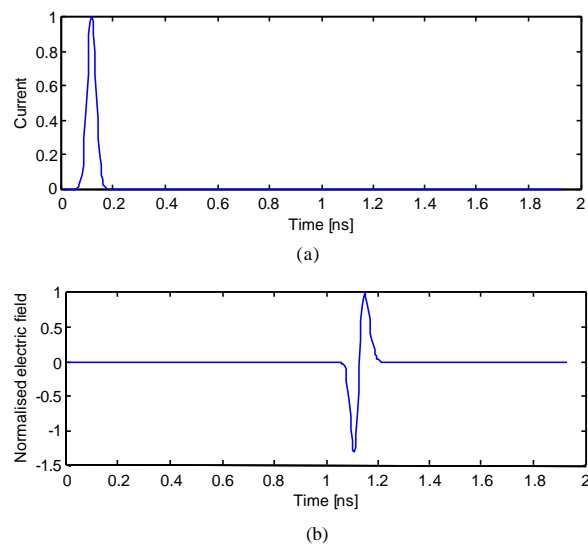
Fig. 3-15: (a) The Gaussian current pulse,

(b) the E_z component on the x-axis at 30 cm from the antenna feed

The surge impedance of the TEM horn

The wire model can also be used to calculate an analytic expression of the surge impedance of the TEM horn. Therefore we first have to calculate the early time electric field in the antenna, which means

$$t < \frac{L}{c} \tag{3.18}$$

In this case all the terms involving r_L vanish and the expression of the electric field in the antenna can be simplified. By definition, the surge impedance can be found from

$$Z = \frac{V(r)}{I_0(t - r/c)} = \frac{-\int_V \vec{E}_{in\,antenna}\,\overline{dl}}{I_0} \tag{3.19}$$

with the integration path V chosen as an arc in the xz plane, so

$$Z = \frac{-\int_{-q_0}^{q_0} \vec{E}_{in\,antenna}\, r\, \vec{a}_q\, dq}{I_0} \tag{3.20}$$

In this model the surge impedance (for L< ∞), and hence the characteristic impedance along an infinite TEM horn (L=∞), is given by [26]

$$Z = \frac{Z_0}{4p} \sum_{i=1}^{N} \left[\ln \frac{1 - \cos j_i \cos 2q_i}{1 - \cos j_i} \int_{j_i - \Delta j/2}^{j_i + \Delta j/2} F(j\,,j_0)\,dj \right] \tag{3.21}$$

with $F(j\,,j_0)$ the azimuth current distribution on the antenna plates, N the number of wires of the wire mesh and j_i and q_i the azimuth and elevation angle of the ith wire. We can see that the surge impedance given by the analytical expression (3.21) is only

function of the angles j_0 and q_0, as we expected. To validate the analytical expression (3.21), we measured the surge impedance of one antenna plate on a ground-plane by time domain reflectometry (TDR) and compared it with the calculated surge impedance. The geometric configuration is the same as shown in Fig. 3-12. The antenna plate has a length of 10 cm and a fixed azimuth half angle j_0 of 30°. The set-up gave the flexibility of changing the elevation angle q_0 very easily.

A TDR measurement generates a step with a short rise-time and measures the reflected signal from impedance discontinuities, to determine the reflection coefficient versus time. From this reflection coefficient, the impedance characteristics versus distance of the device under test is calculated. In our TDR measurements, a step with a rise time of 45ps is used.

For different values of the elevation angle q_0 the surge impedance at the middle of the antenna plate was measured and compared to the values given by (3.21). For the calculation, the number of wires N used in (3.21) was 400. As the measurement was performed on a half TEM horn (one antenna plate on a ground-plane) the measured surge impedance by TDR will be half the surge impedance of a complete TEM horn (two antenna plates). Therefore, the measured surge impedance has to be multiplied by 2. The results are plotted in Fig. 3-16.
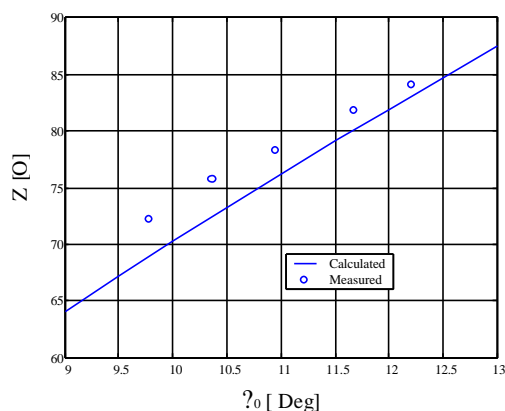
Fig. 3-16: Measured and calculated surge impedance of air-filled TEM horn

Expression (3.21) of the surge impedance given by the wire method turns out to be very accurate for predicting the surge impedance. The wire method slightly underestimates the surge impedance. The maximal discrepancy between the theoretical model and the experimental data is 5%. A quick comparison with the two methods given in Section 3.4.1 learns that this method performs better, and is thanks to its analytical form, flexible for design purposes. The small discrepancy is probably due to the fact that the wave guided by the antenna plates is actually not purely TEM. Higher orders can be introduced by a bad feed at the feed point and of course by edge diffraction.

3.4.3. Design of air-filled TEM horn

In a first part of the thesis, some work was done on the design of air-filled TEM horns. The purpose was not to develop nor to enhance such an antenna, but to validate the wire model. Further we wanted to study the behaviour of the air-filled TEM horn so that its design could serve as a basis for the development of the dielectric-filled TEM horn. We will not go into all the details of the design, but only discuss aspects that are relevant for the dielectric-filled TEM horn. The air-filled TEM horn will nevertheless be used throughout the work to compare with the performance of the dielectric-filled TEM horn.

For the design of a TEM horn, 3 parameters: L, $\boldsymbol{j}_0$ and $\boldsymbol{q}_0$ have to be determined, and this as a function of the user-defined antenna characteristics like fractional bandwidth, antenna pattern, surge impedance, etc.

In this type of antenna, L will mainly influence the lower cut-off frequency and the fractional bandwidth [25][29]. It is not easy to extract a value for L using the discussed models. As a rule of thumb, the length L must be at least half a wavelength of the lowest frequency [4]. We opted for a small antenna with a length L=10 cm. This means a lower cut-off frequency of 1.5 GHz, which is too high according to the design goal stated in Section 3.3.

The first fundamental question is on the impedance of the antenna. In the past, many antenna designers have tried to match the antenna surge impedance at the antenna end to the wave impedance of free space $Z_0 = 120\pi$. In their design they gradually changed the surge impedance from 50 Ω at the antenna feed to 377 Ω at the antenna end by continuously changing along the plates the angles j_0 (flaring out the antenna plates) and/or q_0 (tapering the antenna plates). The aim of the matching is to avoid reflections at the open end of the antenna. In [18] it is shown by simulation and measurement that the concept of matching the surge impedance to that of free space to eliminate reflections is erroneous and that reflections will occur. Further, tapering and flaring out the antenna plates will disturb the TEM mode in the antenna [19] and hence create higher modes. Later on in this work we want to model the antennas in the time domain. In the application of landmine detection, the targets are relatively close to the antennas ($\pm$ 30cm), and these higher modes will make the model less accurate near the antennas.

For these two reasons we have chosen to keep the surge impedance constant over the whole antenna. This means that no tapering or flaring of the antenna plates is used. In the design of the air-filled TEM horn we opted for an antenna impedance of 80 Ω and not for the characteristic impedance of the feed cable, *i.e.* 50Ω, as is usually done for this kind of antenna. The reasons for this will be explained in Section 3.5.1.

An infinite number of couples (j_0, q_0) that yield a surge impedance of 80 Ω are possible, so we have to determine one more parameter. In the design phase of the air-filled TEM horn, we used the wire model to optimise the angle j_0 for a given L and surge impedance of the antenna. As a criterion for the optimisation we looked at the peak-to-peak value of the radiated E-field and the half-power beamwidth. In Table 3-1 a set of couples (j_0, q_0) leading to a surge impedance of 80 Ω is given in steps of 5° for the azimuth angle. The couples are calculated using equation (3.21) in an implicit way.

j_0 [°]	15	20	25	30	35	40	45
q_0 [°]	5.5	7.4	9.5	11.6	14	16.5	19.4

Table 3-1: Couples (j_0, q_0) leading to a surge impedance of 80 Ω

For each couple, the radiated transient electromagnetic field is calculated in the H-plane (*i.e.* the xy-plane in Fig. 3-12) at a radius of one meter from the antenna feed point by equation (3.17). The current pulse used in (3.17) has a Gaussian shape with a Full Width at Half Maximum (FWHM) of 80 ps. This means that the radiated field will be a monocycle as shown in Fig. 3-15 (b). For each of the couples (j_0, q_0) the peak-to-peak value of the radiated E-field (in [V/m]) is plotted on a polar diagram to form a kind of non-normalised radiation pattern (Fig. 3-17).
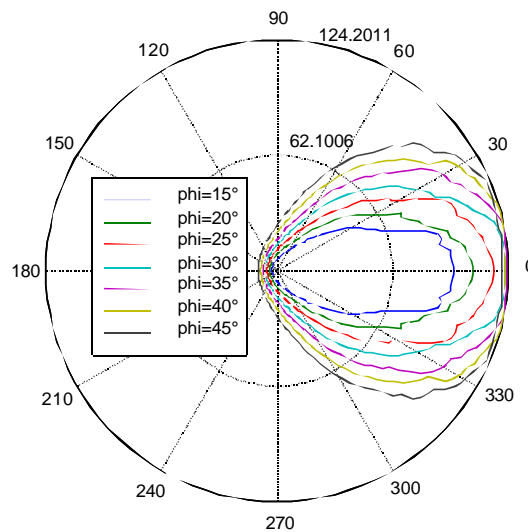
Fig. 3-17: Peak-to-peak value of the radiated E-field in H-plane for different values of j_0

The figure shows clearly a maximum peak-to-peak amplitude on boresight for values of j_0 between 30° and 40°. The maximum is flat, but for $j_0 > 40°$ the peak-to-peak amplitude decreases again and the half-power beamwidth increases. The different values of j_0 and q_0 have little effect on the bandwidth. As a conclusion we can say that the optimal angle j_0 for a surge impedance of 80 Ω, is found to be 30-40 degrees. In our design we opted for $j_0 = 30°$, which leads to an angle $q_0 = 11.2$ (see Fig. 3-16, measured data).

A picture of the air-filled TEM horn is shown in Fig. 3-18. Special attention was paid at the feed-point. The feed point has to be mechanically robust but care must be taken

that it does not introduce a too large impedance discontinuity. A schematic representation of the feed point is given in Fig. 3-19.

Fig. 3-18: Picture of the air-filled TEM horn
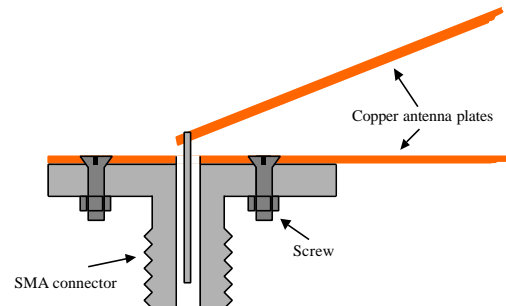
Fig. 3-19 : Schematic representation of the feed point

To validate the wire model, we compare in Fig. 3-20 the measured antenna pattern in the H-plane at 5 GHz with the antenna pattern, calculated by the wire model. The frequency domain measurements were performed in an anechoic chamber in the University of Leuven. For the calculated pattern, we first calculated the radiated E-field in the time domain and then converted to the frequency domain using an FFT. The wire model turns out to be also very accurate in the calculation of the radiation pattern. The 3-dB beamwidth in the H-plane is around 45°. In Fig. 3-21 the $|S_{11}|$ parameter of the air-filled TEM horn is shown (reference impedance is 50 Ω). From the $|S_{11}|$ plot, it can be seen that the TEM horn has a very large bandwidth.
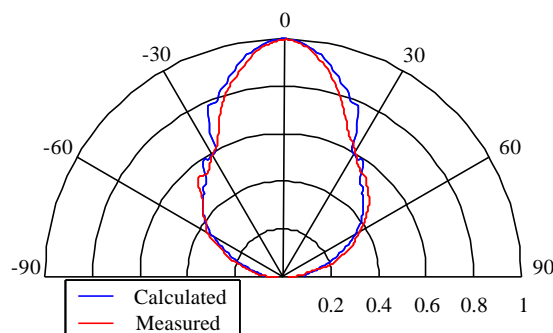
Fig. 3-20: Measured (red) and calculated (blue) antenna pattern in H-plane at 5 Ghz
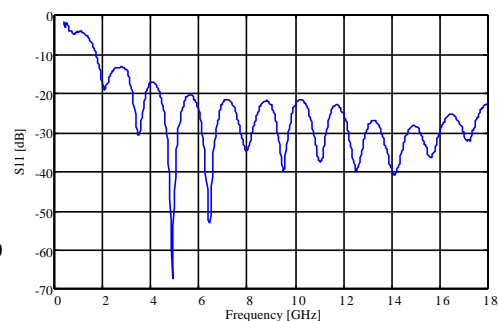
Fig. 3-21: $|S_{11}|$ parameter of air-filled antenna

3.5. Dielectric-filled TEM horn

In order to improve directivity and to reduce the physical size of the antenna without limiting too much the bandwidth, we will fill the TEM horns with a dielectric, characterised by a real relative permittivity e_r and a loss tangent. Thanks to the dielectric, the propagation speed of the TEM wave between the antenna plates will be divided by $\sqrt{e_r}$, in other words, the electrical length of the antenna will be extended by a factor $\sqrt{e_r}$. Further the dielectric filling will reduce the surge impedance of the antenna by approximately a factor of $\sqrt{e_r}$. To preserve the same surge impedance as before the filling, one can increase the angle q_0, which again means an improvement of directivity.

3.5.1. Influence of the filling

The infinite air-filled TEM horn is equivalent to a pure TEM transmission line. Filling this transmission line would result in an inhomogeneous quasi-TEM structure. If this inhomogeneous transmission line becomes of finite length, the structure will be very complex to model and a numerical modeling would be more appropriate. In our approach we based the design on the air-filled antenna and on some principles from micro strip theory.

To study the influence of the filling, the air-filled TEM horn from previous section (L=10cm, j_0=30° and q_0=11.2°) is filled with a silicone, characterised by a real relative permittivity e_r of 2.89 and a loss tangent of 0.0084 at 1 GHz.

Influence on the surge impedance

In the static analysis approximation, used in strip-line theory, the characteristic impedance of a strip-line without dielectric decreases with a factor of $\sqrt{e_{r,eff}}$ when a substrate with a relative dielectric constant e_r is added. The effective relative

permittivity $e_{r,eff}$ is introduced as a correction on e_r by the fact that the structure becomes quasi-TEM after adding the substrate. An expression for the effective relative permittivity as a function of e_r, w the width and h the height of the micro strip is given by Hammerstad and Jensen [24]:

$$e_{r,eff} = \frac{e_r + 1}{2} + \frac{e_r - 1}{2}\left[1 + \frac{10h}{w}\right]^{0.555} \tag{3.22}$$

The effective relative permittivity of the silicone used in the design is calculated using (3.22) as $e_{r,eff}$ = 2,55. According to strip-line theory, the surge impedance of the TEM horn will be reduced by a factor $\sqrt{e_{r,eff}}$ =1,6. The dielectric-filled TEM horn antenna impedance is chosen to match the 50 Ω driving cable so that the part of the transient travelling current that bounces back at the antenna aperture towards the excitation source, will meet no mismatches on its way back. In this way antenna ringing will be avoided. If a filled TEM horn with a surge impedance of 50 Ω is purchased, an empty TEM horn of 80 Ω is needed, which explains the choice of the surge impedance in Section 3.4. Fig. 3-22 shows the surge impedance of the TEM horn before and after the filling. The measurement is done by TDR, using a step with a rise time of 45 ps. The mismatch at the feed point introduced by the connector is small. The reflection coefficient is less than 5%, which means that only 0.25% of the instantaneous transmitted power at the feeding point is reflected back towards the source. The surge impedance along the antenna varies between 45 and 55 Ω, so the reduction of surge impedance due to the filling is indeed found to be the expected $\sqrt{e_{r,eff}}$. Note also that the electrical length of the antenna after filling is extended.
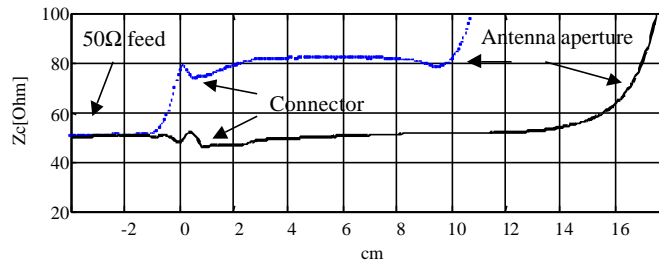
Fig. 3-22: Surge impedance of the TEM horn before (dotted) and after (solid) the filling

Influence on the antenna pattern and the bandwidth

The filling of the antenna will certainly have its effect on the antenna pattern and the frequency band of the antenna. As the electrical length of the dielectric-filled horn is extended, it is expected that the antenna will be more directive and that the lower cut-off frequency will decrease. Fig. 3-23 shows the antenna gain of the air-filled TEM horn and the dielectric-filled TEM horn. The gain is measured in an anechoic chamber using calibrated horn antennas, so losses due to the reflection coefficient of the TEM horn is included in the gain. The whole frequency band of the dielectric-filled TEM horn is reduced (approximately by a factor $\sqrt{e_{r,eff}}$) and has shifted slightly towards the lower frequencies. Fig. 3-24 shows the antenna pattern in the H-plane at 5 GHz. before and after the filling. As expected, the dielectric-filled horn is more directive. This also means that the dielectric-filled TEM horn will be less sensitive to external EM interference, which is an advantage in this application.
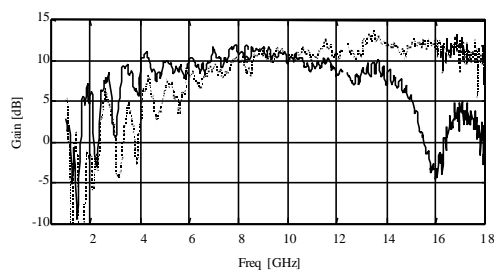
Fig. 3-23 : Antenna gain of the air-filled (dotted) and the dielectric-filled TEM horn (solid)
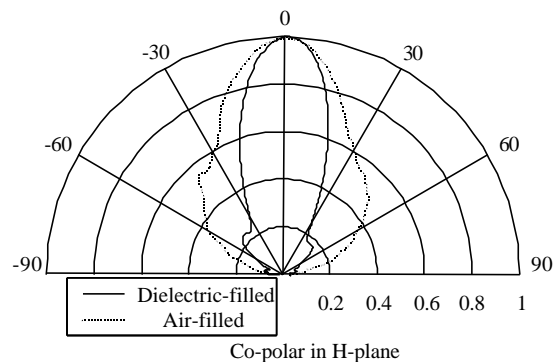
Fig. 3-24 : H-plane pattern at 5 GHz before (dotted) and after the filling (solid)

3.5.2. Design of the dielectric-filled TEM horn

In previous section the air-filled TEM horn was filled with a dielectric to study the influence of the filling. Antenna measurements showed that even after filling the lower cut-off frequency was still too high to meet our design goals. So in a next (and final) design of a dielectric-filled TEM horn we had to increase the length L of the antenna. On the other hand, the antenna's dimensions and weight had to stay limited to guarantee a good mobility of the antennas (see design goals). This means we had to compromise on the length and a length L of 12 cm was chosen.

Further we noticed in previous design a problem with the transition from the unbalanced current in the coax feed cable to the balanced current on the antenna plates. Without precaution an unbalanced current component will be reflected by the antenna feed and appear on the outer conductor of the coax. This current will be the origin of a unwanted TEM mode between the horn conductors and the coax outer conductor. The coax outer conductor will act as an antenna and make the setup sensitive to persons and material in the direct neighborhood of the coax. This situation can be remedied by putting chokes (ferrite cylinders) around the feeding cable. A choke has the following equivalent scheme (Fig. 3-25) and will hence suppress the current pulse on the coax exterior.

Fig. 3-25: Equivalent scheme of choke

Another solution in order to avoid currents on the coax is found in a balun. The problem here is that the balun has to be broad-banded. In literature not many examples of broad-band baluns are found. In [30] some broad-band baluns are proposed, based on the use of ferrite cores. A bandwidth ratio of 20:1 is obtained. In [31] an impedance matching transition from a coaxal line to a balanced two conductor line is accomplished by tapering the outer conductor of the coax towards a line. This

results in a balun with a bandwidth ratio of 100:1, but the balun is too long and not practical to use. In our design we tried out a similar kind of balun. The principle of this balun is based upon an electrostatic reasoning [8]. In a first part of the antenna, an unbalanced configuration of one antenna plate on a ground-plane is imitated (see Fig. 3-26 (a)). The inner conductor of the coax is connected to the upper antenna plate. The currents on the coax outer conductor can only arise from leakage of the field from the upper antenna plate to the coax outer conductor around the edge of the ground-plane. The larger the ground-plane, the smaller the current on the coax outer conductor. This current would be zero for an infinite ground-plane. In the second part of the antenna, the balanced configuration with the two symmetrical antenna plates is achieved (Fig. 3-26 (b)). In between gradual transition from the unbalanced towards the balanced configuration is obtained by tapering the antenna plates (see Fig. 3-27).

(a)   (b)
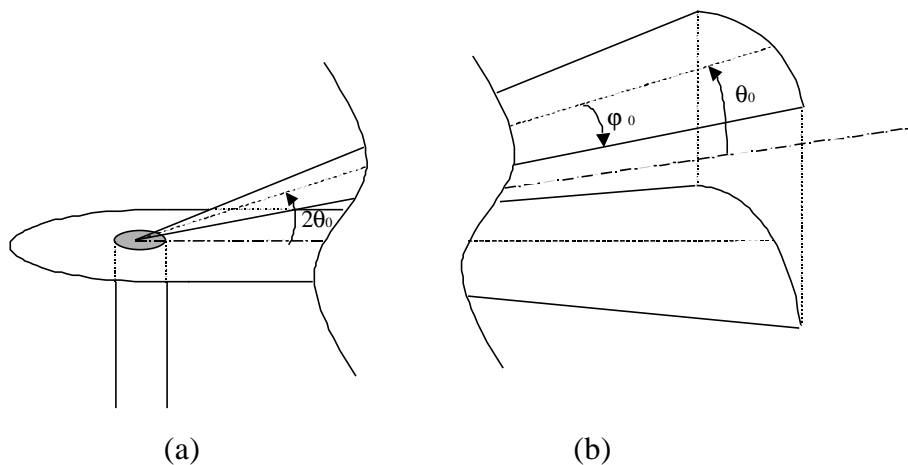
Fig. 3-26: (a) unbalanced configuration (b) balanced configuration

The balun influences the surge impedance of the antenna. The transition from the unbalanced towards the balanced configuration will introduce a slight change in surge impedance along the antenna. Expression (3.21) gives the surge impedance of a complete TEM horn, so in the unbalanced part of the antenna (one antenna plate on a ground-plane), the surge impedance is halve the value given by expression (3.21). But the elevation half-angle (angle between one antenna plate and the symmetry plane of the antenna) is $2q_0$ and not q_0 as in the balanced part of the antenna. The surge impedance of the second part is calculated in a normal way using expression (2.21). In

total, the surge impedance of the unbalanced part is found to be a little inferior to the surge impedance of the balanced part of the antenna.

The antenna impedance of the dielectric-filled TEM horn is chosen to match the 50 Ω driving cable. Doing so, the part of the transient travelling current that bounces back at the antenna aperture towards the excitation source, will meet no mismatches on its way back and antenna ringing will be avoided. The principle seems to work well for frequencies in the band of the antenna. According to the optimal apex half-angle of the air-filled TEM horn (see previous section), the angle j_0 is chosen to be 30° and the physical length L of the antenna plates, as already discussed, will be 12 cm. In this design, the antenna plates are not made out of a copper sheet, but etched on a printed circuit board (PCB). Etching the antenna plates limits the weight of the plates and increases the precision in fabrication. Inspired by the wire model, the antenna plates are replaced by a set of 41 wires (Fig. 3-27). The distance between the wires is too small to influence the antenna characteristics, but it forces the currents to be radial and it limits the surface of conducting metal. The latter is very important, when using the antennas in combination with a metal detector. Etching the antenna plates on a PCB makes it more difficult to create a good and robust feed-point. A schematic representation in Fig. 3-28 shows how the implementation of the SMA connector in the PCB is done.
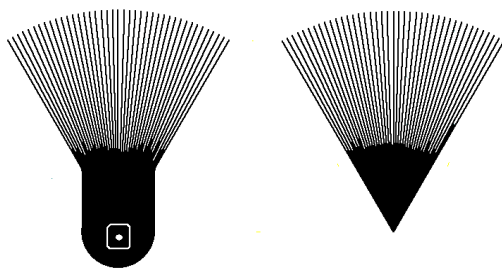
Fig. 3-27: Lower and upper antenna plates, etched on a PCB
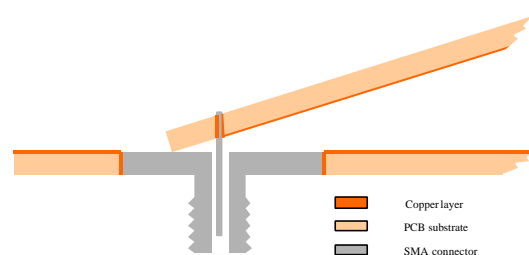
Fig. 3-28: Schematic representation of feed point

Taking into account the reduction of the surge impedance due to the filling and taking into account the influence of the balun, an elevation half-angle q_0 (defined in the balanced part) of 14.5° is calculated to match 50 Ω. This means a surge impedance in the balanced part of 56 Ω. Summarised, we have L=12 cm, j_0=30° and q_0=14.5°, which leads to a physical antenna aperture of 12cm by 6cm.

3.5.3. Results of the dielectric-filled TEM horn

Fig. 3-29 illustrates the surge impedance, measured by TDR, along the antenna. Note that the x-axis is calibrated for speed of light. The gradual transition between the unbalanced part (surge impedance around 55Ω) and the balanced part (surge impedance around 65Ω) is obvious. The reduction of surge impedance due to the filling is again found to be $\sqrt{e_{r,eff}}$. The discrepancy between the measured surge impedance and the wanted one is due to the underestimation of the surge impedance by equation (3.21) (see also Fig. 3-16).
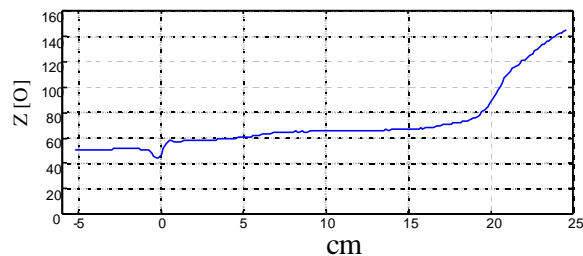
Fig. 3-29: Surge impedance of dielectric-filled TEM horn, measured by time domain reflectometry

Most of the antenna characteristics have been measured in the time domain in the installations of the University of Technology in Delft. In Chapter 4 a more accurate description of the antenna is given under the form of its impulse response. For completeness the $|S_{11}|$ parameter of the antenna is shown in Fig. 3-30. The antenna patterns in H- and E-plane are given in Fig. 3-31. These patterns represent the peak-to-peak value of the radiated impulse in each direction, normalised to one. In this

definition of pattern, **the 3dB beamwidth is 32° in the H-plane and 65° in the E-plane.**
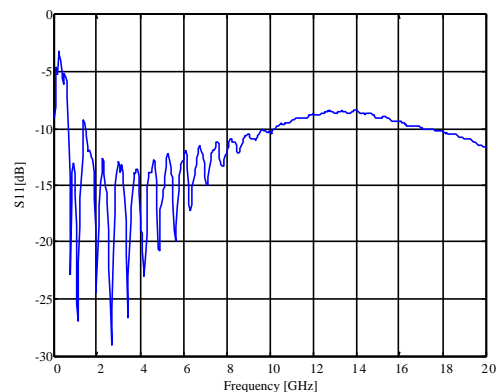
Fig. 3-30 : $|S_{11}|$ parameter of the dielectric-filled TEM horn
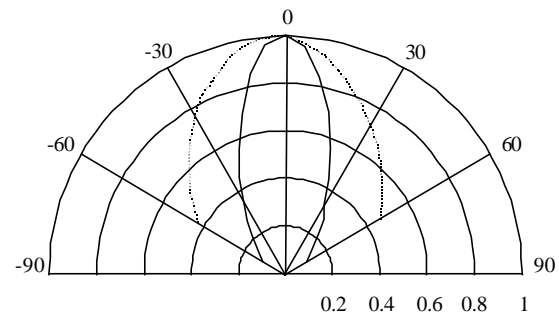
Fig. 3-31 : P-t-p antenna patterns in H-plane (solid) and E-plane (dotted)

Interesting to see, because it is closely related to the application, is the main-beam response of two identical antennas. For this time domain measurement the two TEM horn antennas are aligned on boresight of each other. The transmitting antenna is excited with the Gaussian impulse. The received signal is recorded by a 6 GHz digitising oscilloscope. Fig. 3-32 shows the normalised received voltage as a function of time. At $t < 0.2\,ns$ the recorded signal shows a small negative pre-pulse. This pre-pulse is due to the TEM mode that goes in the opposite way around the antenna plates (see simulation in Fig. 3-14). As this wave travels in free space, it will arrive sooner than the wave that travels between the antenna plates. This negative pre-pulse can be reduced by putting radar-absorbing material (RAM) at the outside end of the antenna plates. The RAM also reduces the low frequency ringing of the antenna as we will see in Section 4.5. Around $t = 1.6\,ns$ the reflection on the antenna end is visible. The signal in Fig. 3-32 is taken with the RAM already on the antenna plates. The frequency band of the whole system (transmitter – antennas - receiver), obtained by a time-frequency transformation of the plot in Fig. 3-32, is from 1 GHz up to 5GHz, so the postulated frequency band of 500 Mhz to 4.5 GHz is not reached.
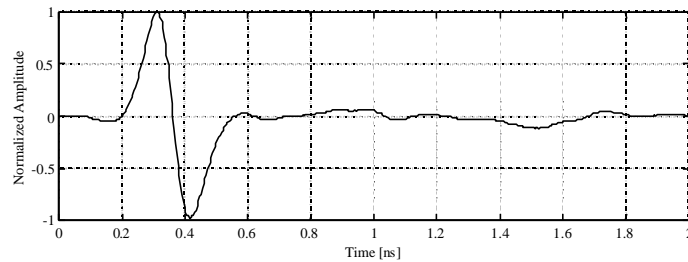
Fig. 3-32: Normalised amplitude of the main beam response

3.6. Summary

In this chapter, we gave an overview of the exiting GPR antennas and UWB antennas, together with some design goals for GPR antennas in the demining application. The TEM horn seemed to be a good candidate to meet these design goals. In a first step an air-filled TEM horn was studied and developed. An accurate model for design purposes was obtained from the wire method. In order to reduce the physical size of the antenna and to improve the directivity, the antenna was filled with a dielectric. Due to the lack of a good model, the design was based on the air-filled antenna, assuming that the antenna guides a quasi-TEM wave. TDR measurements of the surge impedance showed a slight but acceptable difference with the theory. Antenna measurements revealed that the antennas were more directive and that the frequency range moved towards the lower frequencies. The antenna plates were replaced by a set of wires, which makes them suitable for operating in combination with a metal detector. An ultra-wideband balun was also integrated in the antenna plates. Although we are aware that the actual antennas can still be enhanced, most of the design goals are met. The dimensions of the dielectric-filled TEM horns are small, as needed for the application, and they are capable of radiating and receiving very fast transient pulses, without too much ringing, which is of course important for this application. The cleaner the pulse, the cleaner the backscattered signal, and the more easy it will be to post-process and interpret the data. The antennas, that can be used off-ground, are ready to be integrated in an UWB GPR system.

REFERENCES

[1] D. J. Daniels, D. J. Gunton and H. F. Scott, "Introduction to subsurface radar," *IEE Proceedings*, vol. 135, Pt. F, no.4, pp. 278-320, Aug. 1988.

[2] A. A. Lestari, A. G. Yarovoy and L. P. Ligthart, "Adaptive Antenna For Ground Penetrating Radar," *Eight International Conference on Ground Penetrating Radar*, Gold Coast, Australia, pp. 366-371, May 2000.

[3] T. T. Wu and R. W. P. King, "The cylindrical antenna with nonreflecting resistive loading," *IEEE Trans. on Antennas Propagat.*, vol. AP-13, pp. 369-373, May 1965. Correction, p.998, Nov. 1965.

[4] M. Kanda, *Time-Domain Measurements in Electromagnetics*. E. K. Miller, Ed., New York: Van Nostrand Reinhold., 1986, ch. 5.

[5] J. G. Maloney and G. S. Smith, "A study of transient radiation from the Wu-King resistive monopole – FDTD analysis and experimental measurements," *IEEE Trans. on Antennas Propagat.*, vol. AP-41, no. 5, pp. 668-676, May 1993.

[6] T. P. Montoya and G. S. Smith, "A study of radiation from several broad-band loaded monopoles," *IEEE Trans. on Antennas Propagat.*, vol. AP-44, no. 8, pp. 1172-1182, Aug. 1996.

[7] B. Stockbroeck and A. Vander Vorst, "Electromagnetic modes in Conical transmission lines with applications to the linearly tapered slot antenna," *IEEE Trans. on Antennas Propagat.*, vol. AP-48, no. 3, pp. 447-455, March 2000.

[8] V. Rumsey, *Frequency independent antennas.* New York: Academic Press, 1966.

[9] B. Stockbroeck and A. Vander Vorst, "Copolar and cross-polar radiation of Vivaldi antennas on dielectric substrates," *IEEE Trans. on Antennas Propagat.*, vol. AP-48, no. 1, pp. 19-25, Jan. 2000.

[10] R. L. Carrel, "The Characteristic Impedance of Two Infinite Cones Of Arbitrary Cross Section," *IRE Trans. on Antennas and Propagation*, vol. AP-6, pp. 197-201, 1958.

[11] M. Kanda, "Transients in a Resistively Loaded Linear Antenna Compared with those in a Conical Antenna and a TEM Horn," *IEEE Trans. on Antennas Propagat.*, vol. AP-28, no. 1, pp. 132-136, 1980.

[12] M. Piette, E. Schweicher and A. Vander Vorst, "An indoor Time-Domain Measurement System for Studying Transient Radar Signatures of Small Scales 3D-Targets," *RADAR '94*, Paris, pp. 518-522, Mai 1994.

[13] J. G. Maloney and G. S. Smith, "Optimization of a conical antenna for pulse radiation: an efficient design using resistive loading," *IEEE Trans. on Antennas Propagat.*, vol. 41, no. 7, pp. 940-947, July 1993.

[14] C. E. Baum, "Radiation of impulse-like transient Fields," Sensor and Simulation Notes, note 321, Nov. 1989.

[15] E. G. Farr and C. E. Baum, "Prepulse associated with TEM feed of an IRA," Sensor and Simulation Notes, note 337, March 1992.

[16] C. E. Baum and E. G. Farr, "Impulse radiating antennas," *Ultra-Wideband, Short-Pulse Electromagnetics,* C. E. Baum, H. L. Bertoni, L. Carin, L. B. Felsen, Eds., New York: Plenum Press, 1993, pp. 139-147.

[17] M. Kanda, "The Effects of Resistive Loading of TEM Horns," *IEEE Trans. Electromagnetic Compatibility*, vol. EMC-24, no. 2, pp. 245-255, 1982.

[18] K. L. Schlager, G. S. Smith and J. G. Maloney, "Accurate Analysis of TEM Horn Antennas for Pulse Radiation," *IEEE Trans. Electromagnetic Compatibility*, vol. EMC-38, no.3, pp. 414-423, 1996.

[19] A. P. Lambert, S. M. Booker and P. D. Smith, "Transient Antenna Design parameters for optimising Radiated Pulse," Specialists' Meeting on High Power Microwaves, AGARD, Electromagnetic Wave Propagation Panel, *Proc. 54th*, Ottawa, Canada, ch. 8, May 1994.

[20] J. F. Aurand, "A TEM-Horn Antenna with Dielectric Lens for Fast Impulse Response," *Ultra-Wideband, Short-Pulse Electromagnetics 3*, C. E. Baum, L. Carin, A. P. Stone, Eds., New York: Plenum Press, 1997, pp. 113-120.

[21] F. C. Yang and K. S. H. Lee, "Impedance of a Two-Conical-Plate Transmission Line," Sensor and Simulation Notes, note 221, 1976.

[22] F. C. Yang and L. Marin, " Field distribution on a two-conical-plate and a curved cylindrical-plate transmission line," Sensor and Simulation Notes, note 229, 1977.

[23] C. Martel, M. Philippakis and D. J. Daniels, "Time Domain Design of a TEM Horn Antenna for Ground Penetrating Radar," *Millennium Conference on Antennas & Propagation AP-2000*, Davos, Switzerland, vol. II, p. 186, April 2000.

[24] A. Vander Vorst and D. Vanhoenacker-Janvier, *Bases de l'ingénierie micro-onde*. Brussels: De Boeck & Larcier, 1996.

[25] E. G. Farr and C. E. Baum, "A Simple Model of Small-Angle TEM Horns," Sensor and Simulation Notes, note 340, 1992.

[26] J. J. A. Klaasen, "An efficient method for the performance analysis of bounded-wave nuclear EMP simulators," Sensor and Simulation Notes, note 345, 1992.

[27] J. J. A. Klaasen, "An efficient method for the performance analysis of bounded-wave nuclear EMP simulators," *IEEE Trans. Electromagnetic Compatibility*, vol. EMC-35, no. 3, pp. 329-338, Aug. 1993.

[28] G. S. Smith, "Teaching antenna analysis from a time-domain perspective," *Millennium Conference on Antennas & Propagation AP-2000*, Davos, Switzerland, vol. I, p. 435, April 2000.

[29] B. Scholliers, *Studie van de TEM horn antenna*, Eindwerk, Royal Military Academy, Brussels, BE, 1997.

[30] C. L. Ruthroff, "Some broad-band transformers," *Proceedings of the IRE*, pp. 1337-1342, Aug. 1959.

[31] J. W. Duncan and V. P. Minerva, "100:1 bandwidth balun transformer," *Proceedings of the IRE*, pp. 156-164, Feb. 1960.